Auxilliary grid method for the calculation of electrostatic terms in Density Functional Theory on a real-space grid

Journal:	*Physical Chemistry Chemical Physics*
Manuscript ID:	CP-ART-02-2015-001090.R1
Article Type:	Paper
Date Submitted by the Author:	05-May-2015
Complete List of Authors:	Zuzovski, Michael; Tel-Aviv University, Physical Electronics Boag, Amir; Tel-Aviv University, Physical Electronics Natan, Amir; Tel-Aviv University, Physical Electronics

Physical Chemistry Chemical Physics
CREATED USING THE RSC LaTeX PCCP ARTICLE TEMPLATE – SEE www.rsc.org/electronicfiles FOR DETAILS
ARTICLE TYPE www. rsc.org/xxxxxx | XXXXXXXX

Auxilliary grid method for the calculation of electrostatic terms in Density Functional Theory on a real-space grid

Michael Zuzovski,[a] Amir Boag,[a] and Amir Natan[a*]

Received Xth XXXXXXXXXX 20XX, Accepted Xth XXXXXXXXX 20XX
First published on the web Xth XXXXXXXXXX 200X
DOI: 10.1039/b000000x

In this work we show the implementation of a linear scaling algorithm for the calculation of the Poisson integral. We use domain decomposition and non uniform auxiliary grids (NG) to calculate the electrostatic interaction. We demonstrate the approach within the PARSEC Density Functional Theory code and perform calculations of long 1D carbon chains and other long molecules. Finally, we discuss possible applications to additional problems and geometries.

1 Introduction

Density Functional Theory (DFT)[1] has become the method of choice for the calculation of the electronic properties of large systems, this is mostly because of a good balance between numerical accuracy and computational cost. In most applications, the Kohn-Sham (KS)[2] differential equations are solved either by a basis representation such as Gaussian basis sets[3], local numerical basis sets[4], plane waves[5–7], or wavelets[8] or via the representation of the wave function over a discrete grid[9–15]. While each method has its own advantages and disadvantages, the use of a discrete grid, also known as the real-space method[9,10,12] has some advantages for parallel implementations of large systems[16,17]. Another advantage of the real-space method is that it is relatively straightforward to use the Runge-Gross theorem for time dependent DFT (TDDFT)[18] and perform direct time propagation of the KS orbitals (RT-TDDFT)[13,19,20]. Both for ground state and especially for the time dependent case, the calculation of the electrostatic interaction term, known as the Hartree potential, and the Fock exchange interaction term , is becoming the most time consuming part of the problem. The Hartree term is given by:

$$V_H(\vec{r}) = \int \frac{\rho(\vec{r}_1)d\vec{r}_1}{|\vec{r}-\vec{r}_1|} \tag{1}$$

As the direct calculation of the integral given in Eq. 1 is of $\mathcal{O}(N^2)$ complexity, where N is the number of grid points, most implementations solve instead the equivalent Poisson equation:

$$\nabla^2 V_H(\vec{r}) = -4\pi\rho(\vec{r}) \tag{2}$$

Eq. 2 is conventionally solved with iterative solvers such as the conjugate gradient (CG)[21] or multi-grid solvers[15,22,23]. Another approach is to use the Fast Fourier Transform (FFT)[24,25] to calculate V_H. Both CG and multi-grid solvers require the formulation of boundary conditions. For many situations, the multipole approximation[26], is a good and efficient way to set the boundary conditions of the system but for structures with high aspect ratio there are known convergence issues and so either a larger box should be taken or a much slower calculation for the boundaries should be used. With FFT the box size should be twice the size of the system in each dimension, which also makes the calculation slower. The appearance of efficient algorithms such as the Fast Multipole Method (FMM)[27,28] makes it possible to re-consider the direct calculation of Eq. 1. In recent years, FMM based[29–32] and other[33–36] efficient integration methods were implemented for Hartree and Fock exchange terms in quantum calculations. In this work we present a method, based on auxiliary non-uniform grids (NGs)[37,38], that can asymptotically reach $\mathcal{O}(N)$ performance. The NG method uses FMM-like hierarchical domain decomposition to compute Eq. 1, but represents the potentials by their values on non-uniform auxiliary grids which are then used for interpolation to an arbitrary grid. The rest of the manuscript is organized as follows: we first review the real-space method as implemented in the PARSEC code and then describe the NG algorithm. We discuss some important implementation details, with a particular emphasis given to elongated structures. Finally, we present results, demonstrating the algorithm's performance, for ground state calculation of 1D carbon chains. We conclude with some discussion of how this method can be used for additional geometries and also for Fock Exchange and screened exchange calculations.

[a]*Department of Physical Electronics, Tel-Aviv University, Tel-Aviv, Israel*
[*]*Amir Natan, Tel: +972-3-6408635; E-mail: amirnatan@tau.ac.il*

2 Brief introduction of the Real-Space pseudopotential method

The real space pseudopotential method is based on sampling the orbitals on a uniform grid and on converting the KS differential equations to high order finite difference equations. We write first the spin un-polarized KS equations as:

$$\left(-\frac{\nabla^2}{2}+\hat{V}_{ion}(\vec{r})+V_H(\vec{r})+V_{XC}(\vec{r})\right)\varphi_m(\vec{r})=\varepsilon_m\varphi_m(\vec{r})$$
$$\rho(\vec{r})=2\sum_{m=1}^{Nocc}|\varphi_m(\vec{r})|^2 \quad (3)$$

where we use atomic units throughout, ε_m and φ_m are the eigenvalues and eigenvectors of the equation respectively, and $\hat{V}_{ion}$ is the ionic potential, calculated using the pseudopotential method as described in [9,10]. V_H is calculated via the solution of Eq. 2 and finally V_{XC} is calculated according to the selected functional. The Fornberg [39] formulation of high order finite difference is used to write:

$$\frac{\partial^2\varphi_m(x_i,y_j,z_k)}{\partial x^2}=\sum_{n=-D}^{n=D}\frac{C_n}{h^2}\varphi_m(x_i+nh,y_j,z_k)+\mathscr{O}(h^{2D}) \quad (4)$$

where h is the mesh size and C_n are the finite difference coefficients. Doing so to all partial derivatives, the Laplacian is now represented by a high order finite difference discrete operator. This representation is then used in both Eq. 3 and Eq. 2 self consistently. The resulting finite difference equations are then solved as described in [9,10]. To solve Eq. 3 in a finite domain the wave functions, φ_m, are restricted to be zero outside the domain and the KS equations are solved over that domain. While we focus in this work on finite systems, the same method can be used for 1D [40], 2D, and 3D [41] periodic calculations by applying the appropriate Bloch conditions. To solve the finite difference form of Eq. 2 for non-periodic systems, the conjugate gradient (CG) method is used with appropriate Dirichlet boundary conditions for the potential that can be calculated via the multipole expansion and other methods.

3 Algorithm description

3.1 Discrete form of integral summations

We now focus on strategies for calculating the Hartree term. We first discuss the relationship between the continuous integral, given in Eq. 1, to its possible discrete form approximation. A naïve approximation to the integral would be:

$$V_H(x_i,y_j,z_k)=\int\frac{\rho(\vec{r}_2)d\vec{r}_2}{|\vec{r}_{i,j,k}-\vec{r}_2|}\approx h^3\sum_{m,n,l}\frac{\rho(x_m,y_n,z_l)}{|\vec{r}_{i,j,k}-\vec{r}_{m,n,l}|} \quad (5)$$

The summation in Eq. 5 assumes $(m,n,l)\neq(i,j,k)$. The self-contribution term, $(m,n,l)=(i,j,k)$, has to be found analytically or numerically and depends on the grid interpolation kernel. However, the approximation in Eq. 5 is too crude in comparison to solving the high order finite difference Poisson equation and would require a very fine grid to converge. This is because the potential of a volume element of charge is not given by $\frac{\rho(x_m,y_n,z_l)}{|\vec{r}_{m,n,l}-\vec{r}_{i,j,k}|}$. The difference is significant mostly for the immediate neighbors, we can therefore try to replace the $1/r$ Green's function by the true potential of the volume elements at the centers of neighboring elements. While there are analytic forms for the electrostatic potential of a cube, we made the choice of using the finite difference Poisson equation to calculate the potential of a point charge located at the origin and to use this potential for the values of the Green's function. And so instead of calculating Eq. 5, we calculate:

$$V_H(x_i,y_j,z_k)\approx h^3\sum_{m,n,l}\rho(x_m,y_n,z_l)G(\vec{r}_{i,j,k},\vec{r}_{m,n,l}) \quad (6)$$

where $G(\vec{r}_{i,j,k},\vec{r}_{m,n,l})\underset{\Delta r\gg h}{\rightarrow}\frac{1}{|\vec{r}_{i,j,k}-\vec{r}_{m,n,l}|}$ is the corrected interaction, $\Delta r\equiv|\vec{r}_{i,j,k}-\vec{r}_{m,n,l}|$ and h is the grid spacing. While Eq. 6 gives a better approximation for the Hartree potential, it would still take $\mathscr{O}(N^2)$ to calculate and therefore some additional approximations should be made.

3.2 Multipole approximation and Non uniform Auxiliary grid

In this section we review the algorithm of building a Non Uniform Auxiliary grid (NG) that was developed for fast calculation of capacitance of complex systems [37]. The first part of the algorithm follows the FMM logic, but we write it here for completeness. To get some approximate, but more efficient calculation, we first note that for any set of point charges in space we can use the multipole expansion [26] and so write the potential of charges that are located in a volume Ω around the origin as:

$$V_\Omega(\vec{r}_{i,j,k})=\sum_{m_1=0}^{\infty}\sum_{m_2=-m_1}^{m_2=m_1}\frac{f(m_1,m_2)}{|\vec{r}_{i,j,k}|^{m_1+1}}Y_{m_1}^{m_2}(\theta,\phi) \quad (7)$$

where $f(m_1,m_2)$ is the (m_1,m_2) moment of the charge and $Y_{m_1}^{m_2}$ are the spherical harmonics. Far enough from the charge volume, the expression in Eq. 7 can be truncated to a finite summation up to order T : $V_\Omega^T(\vec{r}_{i,j,k})\approx\sum_{m_1=0}^{T}(\cdots)$, while keeping a small relative error E_{rel}. If the charges can be assumed to be all contained in a sphere of radius R_S, a closed form expression can be obtained for the truncation order that is needed to get a given maximal relative error. At a distance R from the system, we would get [37]:

$$T \geq \log_{R/R_S}(E_{rel}^{-1}) - 1 \quad (8)$$

Eq. 8 encapsulates the basic idea - that the truncation order, for a desired value of relative error, depends only on the ratio R/R_S. If we define a far-field potential as one for which $R > W \cdot R_S$, i.e. the criteria for using the approximation scales linearly with the domain size, we can divide the space in a multi-level decomposition to blocks of varying size, R_S, while the basic mathematical form of the far-field potential of each block, at any level, remains the same.

Next, we would like to build a method that would allow us to sample expression (7) and so use a cheaper interpolation scheme for the potential at other arbitrary grid points. At this point we deviate from traditional FMM and build the auxiliary grids. Expression (7) consists of elements of the form $r^{-a}e^{ib\theta}e^{ic\phi}$ with $1 \leq a \leq T+1, -T \leq b,c, \leq T$. Thus, we can sample $T+1$ equally spaced points in the $\alpha \equiv r^{-1}$ variable and $2T+1$ in each of the angular coordinates variables, to fully reconstruct V^T from the samples. We also note, that for larger R, it is evident from Eq. 8 that we can use a smaller T and hence less angular sampling points. The reconstruction is done using a polynomial interpolation in the α variable and an interpolation filter in the angular coordinates[37].

So far, we have treated the far-field potential of a single volume and have devised an α grid that enables us to interpolate the potential. The α grid is uniform in r^{-1}, but non-uniform in r. The grid thus formed with the radial and angular variables is a Non-uniform auxiliary Grid which we call NG. Note that although there are codes that solve the KS equations themselves on a non-uniform grid[14,42,43], the idea here is different - we use many auxiliary non-uniform grids for the purpose of electrostatic potential interpolation. In a typical situation of decomposition of space, we would like to gather the far-field potential of many distinct domains at a given domain. To that end, we devise a new local grid that will allow us to interpolate the far-field contribution of several sources. This local grid is illustrated in Fig. 1.

In this construction, we build a grid that is uniform in all co-ordinates and has a total number of grid points that is also independent of system size for a given required relative error. In practice, we use sampling that is denser than the theoretical requirements to allow for a linear interpolation of the potential from its samples, which reduces the total complexity. Also, the potential at the sampling points is at first constructed using the exact, discretized integration form, Eq. 6, and not the truncated multipole expression, and the values that are sampled on the grid are of the function $rV(\vec{r})$, which is a smoother function and is less prone to numerical issues. Once an appropriate local grid is defined, we can divide the problem space into domains of varied size, R_S, such that a multi-level hierarchical decomposition is built. In this scheme, we keep track of parent-child relation (blocks of level i contain blocks of level $i+1$, the level being higher meaning smaller blocks). We define two domains to be well-separated if their distance, R_d, fulfills $R_d > W \cdot R_S$. Domains that are not well-separated will be called neighbors. We can now define, in a similar fashion to the FMM algorithm, the 'Interaction List' of a domain j, as the set of all domains which are well separated from j, while their parents are not well separated from the parent of j. This concept is illustrated in Fig. 2.

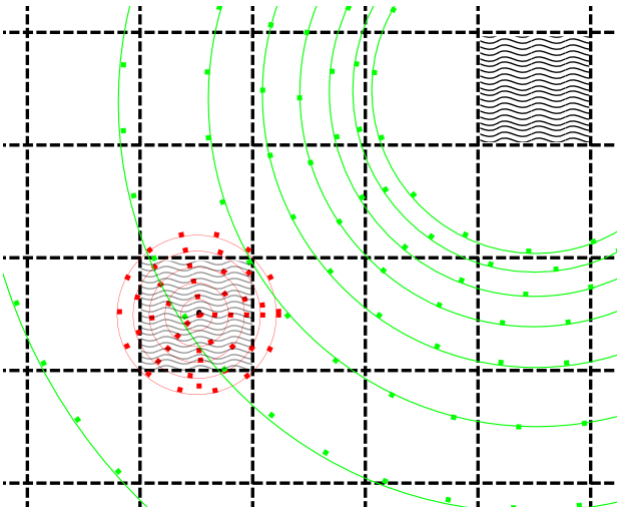

Fig. 1 The far field grid (Green), and the local grid (red) of the upper and lower wave-filled blocks, respectively (given $W = 2$).

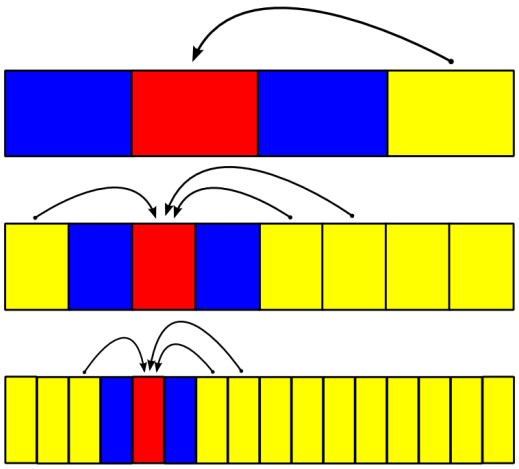

Fig. 2 A 1D illustration of different levels. The cell of interest is shown in red, the near neighbors in blue and the interaction list are the yellow cells with arrows. The arrows show how the interaction list data is interpolated into the cell - this is discussed later in the text.

3.3 Algorithm details

We now describe how by the combination of hierarchical decomposition and far field interpolation we calculate the electrostatic potential. In a general 3D problem, with a cubic domain, we divide space into 8 cubes and then repeatedly divide each cube into 8 child cubes until we reach the minimal allowed domain size which can be 1 grid point or bigger. We define level 0 as the whole problem domain and call it the highest level. Level 1 will have 8 cubes and so on. For simplicity, we have assumed that our domain is a cube of size $2^N \times 2^N \times 2^N$ - this assumption is not necessary as we can play with the minimal domain size and also add zeros to a more general box. While the algorithm can be implemented in 3D as described above and in [37], we have made the choice of considering first elongated structures where our box is of size $L_x \times L_y \times L_z$ and we have $L_z \gg L_x, L_y$. To demonstrate the algorithm scaling with L_z, we made the simplification of performing domain decomposition only along the z axis, such that the angular sampling in θ, ϕ can be approximated by sampling in the x, y co-ordinates, and the interpolation of the potential at any point (x, y, z) can be made simply by only using points with the same (x, y) co-ordinates. These simplification still improves the algorithms' numerical complexity while yielding an acceptable numerical error.

The algorithm is now defined as follows:

- hierarchical domain decomposition.
- At the lowest level, calculate the exact potential on the far field NG grid and near neighbor potentials.
- Up-tree stage - For each level - build a far field NG grid for each domain by interpolation of the child domains $V_{far}(i) = \sum_{j \in children(i)} interpolation(V_{far}(j))$ - the interpolation is needed because the NG grids of the domains are not the same.
- We now use a Down-tree pass to sum the contribution of different blocks. Starting from level 2 we take each block Interaction List (IL) domains and interpolate their far-field NG values into the block local grid. From level 3 and lower we add also the contribution of the domain's parent grid potential. And so:

$$V(Block(k)) = \sum_{i \in IL(k)} Interp(V_{far}(i)) + Interp(V_{inner}(parent(k))) \quad (9)$$

The last stage can be illustrated by figure 2. At the end of the last stage we get the potential at every grid point.

4 Scaling and results for some model systems

4.1 Scaling tests for the algorithm

We first checked the performance of the algorithm on a synthetic problem where we have produced a charge density and compared speeds of a direct calculation to the NG implementation. We took a box of $8 \times 8 \times L_z$ points with L_z going till 600, and compared the speeds as shown in figure 3.

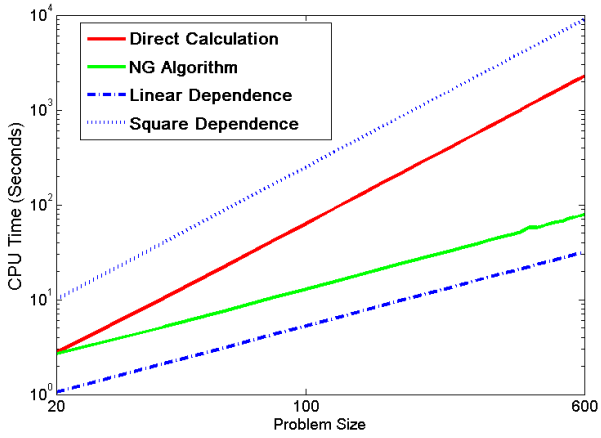

Fig. 3 Comparison of direct calculation of integral (shown in red) to the NG algorithm (shown in blue)

Fig. 3 clearly shows linear scaling compared to the cubic scaling of a direct calculation. It should be noted that since we have performed the hierarchical decomposition only in one dimension this is still not very efficient as the scaling is $\mathcal{O}(n_x^2 n_y^2 n_z)$. To reach the full efficiency one needs to do the decomposition in all dimensions - this was done in [37] for electrostatic applications and was further implemented on GPUs [38] to get additional acceleration. In those works they report scaling values reaching $\sim 400N$ behavior for practical applications. FMM and other implementations have also reported $\mathcal{O}(N)$ and $\mathcal{O}(N \log(N))$ complexities. FFT based works [24,25] report $\mathcal{O}(N \log_2(N))$, however, the FFT constant is 5 and since $\log_2(N = 10^6) \sim 20$ it can reach better performance on a regular grid. A possible advantage of both the NG method and FMM like methods is that they can reach significantly better performance when the charge density becomes sparse, furthermore the NG method can easily be adapted to screened potentials, other kernels and also to work with codes that solve the KS equations on non-uniform grids.

An additional consideration is memory, the NG main memory requirement is coming from the non-uniform auxiliary grids at the lowest level, this is $\mathcal{O}(N)$ with a constant that depends on the chosen size of α grid and the lowest level block size. The algorithm accuracy is controlled by the density of the

NG and the size of the smallest domain. As the algorithm is implicitly based on the truncation of the multipole expansion, the errors in potential estimation can in some cases accumulate in the total energy expression, this makes the convergence tougher (higher T and therefore denser NG grid). However, the eigenvalues and changes in total energy (e.g. due to ionization or geometry change) converge much faster. The convergence can be significantly improved by calculating the local ionic term also with the NG method as some of the possible truncation errors will cancel out.

4.2 Simulation of 1D carbon chains

A simple test case for an elongated structure is that of 1D chains of carbon, also known as carbyne. Such chains can appear in two forms[44], one called cumulene, where the carbons in the chain are equi-distant and have a double bond $(=C=C=)_n$, and the other called polyyne where there are alternating single and triple bonds $(-C\equiv C-)_n$. To test our approach we have calculated $H(-C\equiv C-)_nH$ with n=40 and n=110 and verified that the eigenvalues we get with CG and with NG are the same. We have used a box of $12a.u.\times 12a.u.\times 160a.u.$ and also a box of $12a.u.\times 12a.u.\times 320a.u.$ While it is possible to calculate with a thinner box - it results in wrong eigenvalues as the confinement of the wavefunction becomes too unrealistic. In all calculations we have used grid spacing of $0.4a.u.$ We have also calculated the periodic case, $(-C\equiv C-)_n$, as in[44] for a cell of $5.159a.u.$ and $18.8973a.u.(10\mathring{A})$ in the other dimensions. We have used norm conserving pseudopotentials of s/p cutoff radius (a.u.) of $C:1.6/1.6$ and $H:1.39$. The periodic calculations were compared to plane-waves calculations with PAW pseudopotentials that were done with the VASP code[5]. In addition to the case of 1D polyyne chains, we have calculated also additional examples (shown in Appendix B) of Alkyl chain of length 40 - $C_{40}H_{82}$, polar poly-pyrimidine chains of length 10 and 20 ($(C_4N_2H_2)_nH_2$) units and alpha helix configuration of poly-glycine with 40 amino acids, $C_{80}H_{122}N_{40}O_{41}$. The peptide example is a bit artificial as peptides of such length tend to fold unless the edges are held by some other structure. Both the poly-pyrimidine and poly-glycine are examples of polar chains with polar subunits that accumulate a significant dipole for the whole chain. The gap in polymers generally gets smaller as the chain gets longer, this is further enhanced by the polar interaction as was demonstrated for the poly-pyrimidine case[45].

4.2.1 Periodic case To describe the periodic case we have used a periodic cell of $5.159a.u.$ length in the periodic direction and $18.8973a.u.(10\mathring{A})$ periodicity in the other dimensions. The cell is drawn in Fig. 4. As described in[44], the distances between the atoms are $2.8535a.u.(1.51\mathring{A})$ for the single bond and $2.3055a.u.(1.22\mathring{A})$ for the triple bond.

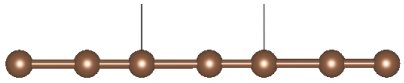

Fig. 4 Unit cell of 1D C chain. The cell boundaries are indicated by the vertical lines.

We have calculated the band structure of the cell and compared the results of the plane-waves calculation to the real-space calculation as shown in Fig 5.

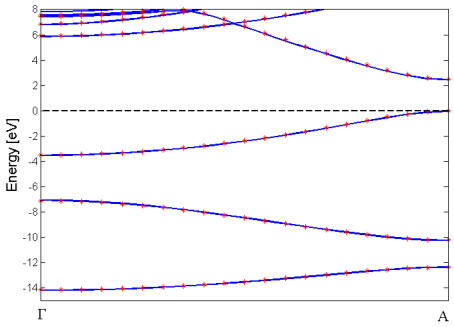

Fig. 5 Band structure of 1D carbon polyyne chain, the solid blue lines are plane waves calculations, the red asterisks are results of the PARSEC code. The Fermi level is shown at the top of the valence band by dash-dotted black line.

4.2.2 Finite carbon chains Next we have calculated the properties of $H(-C\equiv C-)_{20}H$. We took the bulk distances and calculated the electronic properties without further relaxation. The cell and structure of the $H(-C\equiv C-)_{20}H$ are shown in Fig. 6.

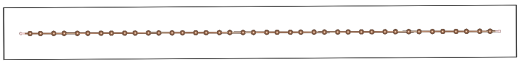

Fig. 6 $H(-C\equiv C-)_{20}H$ structure, the box is shown for proportions.

We have terminated the chain with hydrogens at a bond distance of $2.0598a.u.(1.09\mathring{A})$. An interesting thing to note is that already at $n=20$ (40 C atoms) the electronic eigenvalues are already very close to the bulk state. We have compared the eigenvalues of the finite $n=20$ case with the eigenvalues of a periodic k-grid of 20 points, using the fact that the band is monotonic, we have aligned the eigenvalues according to their order. This is shown in Fig. 7 for the valence band. Such a behavior, of a finite system approaching the properties of the infinite polymer is known for both this and other systems[46,47]

We have examined the effect of neighbor correction, described earlier, on the resulting eigenvalues, where we have compared the solution of CG with the NG algorithm with

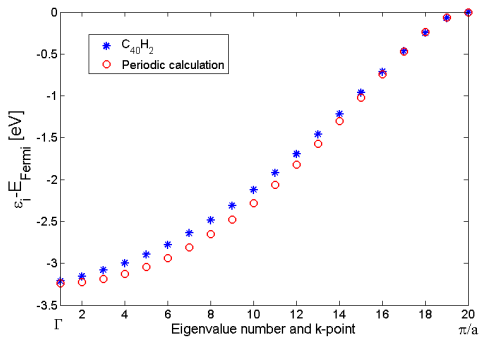

Fig. 7 Comparison of periodic (red circles) and $H(-C\equiv C-)_{20}H$ (blue asterisks) electronic eigenvalues in the valence band, eigenvalues are shown with reference to the Highest Occupied Molecular Orbital (HOMO) or E_F, so the top occupied state is 0

and without 4^{th} nearest neighbor correction as shown in Fig. 8. As is evident, the neighbor correction scheme is critical for getting the correct eigenvalues. We have also calculated and $H(-C\equiv C-)_{55}H$ and reached box size of $12a.u.\times 12a.u.\times 320a.u.$ To test the algorithm, we also went to box size of $1000a.u.$ and still managed to get correct behavior of the solver. To check our calculations with non neutral systems we have removed 1 and 2 electrons and compared the difference in Total energy for both the CG and NG calculations, the difference in ionization energy was 0.003Ry and 0.005Ry respectively, representing a relative error of ~ 0.005 in ionization energy.

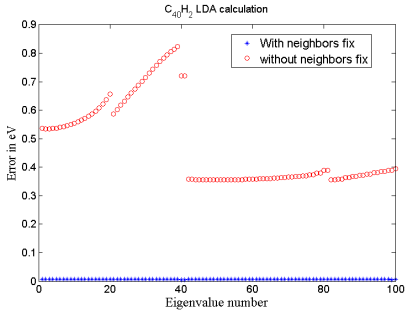

Fig. 8 Effect of neighbor correction scheme. The error in eigenvalues relative to a CG calculation, is shown for 4 neighbors correction (blue asterisks) and without neighbor correction (red circles).

5 Summary

We have shown an auxiliary grid method for the calculation of the electrostatic terms in DFT. We have also shown that we get a linear scaling for elongated structures and also demonstrated the accuracy with a system of 1D carbon chains and other long molecules. While we have demonstrated the method for the ground state Hartree term, it is easy to show that the same method can be used to calculate the Fock exchange pair integrals and also the Hartree term in time dependent problems. The main advantage of the method is that it allows the use of minimal box. In elongated structures and also in quasi-planar structures (e.g. very large graphene nano ribbons) this can be very helpful as the usual multipole approximation does not converge for high aspect ratio domains and so it is difficult to efficiently set the boundary conditions for Poisson equation solvers (either CG or multi-grid). The NG scheme can also be used as a method to calculate the boundary conditions for such solvers. An important situation where the NG method (or other FMM based methods) can be even more efficient relative to other methods is when the structures are low dimensional though not linear or planar but curved - A curved 1D or 2D structure can occupy an even larger encompassing box, making the use of FFT slower. An additional possible advantage of the method, common also to other integration based methods, is that we can easily estimate regions where either the charge density or the potential are zero or close to zero - in some cases the calculation is not needed at all at those points (either for the source charge or for the potential or both) and so a significant reduction in time can be achieved. Finally, it is also possible to tailor the grid interpolation scheme to other interaction kernels, e.g. screened potentials, with such potentials we expect better performance as the far field behavior is almost trivial.

Acknowledgements

AN wishes to acknowledge support from ISF grant 1722/13. AB wishes to acknowledge support from ISF grant 1081/12.

Appendix A - Calculation of ionic potential

The electrostatic potential in Eq. 3 is composed from the V_H term, arising from the electron density, and the ionic term. Naively, it possible to write the ionic potential of a nucleus with Z protons as $V_{ion}(\vec{r}) = -\frac{Z}{|\vec{r}-\vec{R}|}$. However, this potential is often replaced with a softer pseudo-potential that includes the core electrons and is much smoother near the origin. In the PARSEC code, norm-conserving pseudopotentials[48] are used, and the Kleinman-Bylander method[49] is used. This makes the ionic potential a non local operator that is represented as follows:

$$\hat{V}^a_{ps}\varphi_n(\vec{r}) = V^a_{loc}(r_a)\varphi_n(\vec{r}) + \sum_{l,m} G^a_{n,lm}\tilde{u}_{lm}(\vec{r}_a)\Delta V_l(r_a) \qquad (10)$$

Where $\vec{r}_a = \vec{r} - \vec{R}_a$, $r_a = |\vec{r}_a|$, and $\tilde{u}_{lm}(\vec{r}_a)$ is the atomic pseudo wave function corresponding to angular momemntum lm and the projection coefficients are given by:

$$G^a_{n,lm} = \frac{1}{< \Delta V^a_{lm} >} \int \tilde{u}_{lm}(\vec{r}_a) \Delta V_l(r_a) \varphi_n(\vec{r}) d^3 r \qquad (11)$$

with:

$$< \Delta V^a_{lm} >= \int \tilde{u}_{lm}(\vec{r}_a) \Delta V_l(r_a) \tilde{u}_{lm}(\vec{r}_a) d^3 r \qquad (12)$$

Above the cutoff radius, R_c, we have $\Delta V_l(r_a) = 0$ and $V^a_{loc}(r_a) = -Z_{ps}/r_a$ where Z_{ps} is the total charge of the nucleus and core electrons. The total ionic potenital is then calculated by a summation over all ions in the system:

$$\hat{V}_{ion} = \sum_a \hat{V}^a_{ps} \qquad (13)$$

Equation 13 is used exactly as is in finite systems which are the focus of this work. For completeness we describe shortly also the 3D and 2D implementations. In 3D we use the Ewald summation technique[12] to calculate the ionic potential. While in 2D it is possible to use 2D forms of the Ewald summation[12,50] we have chosen[41] a different approach[51] - we add and subtract positive gaussian charges to the ions to separate the potential into long and short range parts. The positive charge is given by: $n_+(r_a) = (\gamma_a/\pi)^{(3/2)} Z_{ps} \exp(-\gamma_a^2 r_a^2)$, the potential of such charges is given by: $V_+(r_a) = -Z_{ps} erf(-\gamma_a r_a)/r_a$. We can then represent the local potential from Eq. 10 as:

$$V^a_{loc}(r_a) = \Delta V(r_a) + V_+(r_a) \qquad (14)$$

The first term in Eq. 14 can be shown to decay very fast[51] and hence can be easily calculated by direct summation of few neighbors. The second term can be calculated by solving the Poisson equation with 2D boundary conditions[41]. It is possible to use this method also for finite systems and to calculate the electrostatic potential of the gaussian charges plus the electron density. This has minimal additional computational cost and has the advantage of reducing the residual errors of truncated multipole expansions because now it is calculated for locally neutral domains.

Appendix B - Additional examples

Alkyl chain $C_{40}H_{82}$

We have used an alkyl chain of 40 units. As before we have used norm conserving pseudopotentials of s/p cutoff radius (a.u.) of $C : 1.6/1.6$ and $H : 1.39$. Grid spacing of $0.4 a.u.$ and a box of $20 a.u. \times 20 a.u. \times 140 a.u$. The system is described in

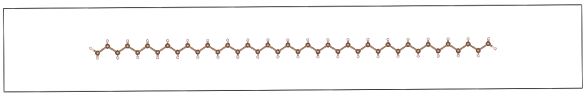

Fig. 9 Alkyl chain with 40 units

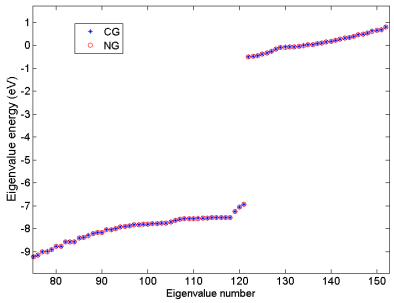

Fig. 10 $C_{40}H_{82}$ eigenvalues. The CG results are shown with blue asterisks, the NG results are shown by red circles. The lower line is the top of the occoupied states. The upper line is the start of empty states.

Fig. 9. The CG band-gap is $6.4143 eV$ compared to $6.4141 eV$ of NG. Some of the eigenvalues are shown in Fig. 10, and show very good agreement between the two methods.

Poly-pyrimidine

We have calculated the dipole and band gap of both 10 and 20 units poly-pyrimidines ($(C_4N_2H_2)_nH_2$). We have used norm conserving pseudopotentials of s/p cutoff radius (a.u.) of $C : 1.6/1.6$, $N : 1.5/1.5$, and $H : 1.39$. Grid spacing of $0.4 a.u.$ and a box of $20 a.u. \times 20 a.u. \times 160 a.u.$ for the 10 units and $20 a.u. \times 20 a.u. \times 200 a.u.$ for the 20 units. The 10 units system is shown in Fig. 11. For the 10 units the CG dipole was $23.074 D$ compared to $23.086 D$ with NG (diff. of $\sim 0.01 D$). The CG band gap was calculated to be $1.6821 eV$ compared with 1.6809 of NG (diff. of $\sim 0.001 eV$). For the 20 units system the CG dipole was calculated to be $42.3804 D$ while the NG was $42.387 D$ (diff. of $0.006 D$), the CG band gap was $1.4783 eV$ compared to $1.4757 eV$ of NG (diff. of $0.0026 eV$). Those LDA values are slightly lower the PBE values calculated elsewhere[45] but show very similar trends.

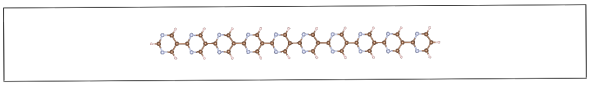

Fig. 11 Poly-pyrimidine with 10 units. Box size is $20 a.u. \times 20 a.u. \times 160 a.u.$, carbon atoms are shown in brown, hydrogen in white and nitrogen in light blue

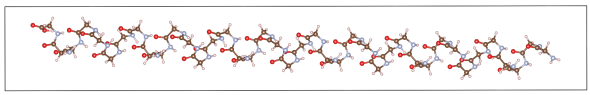

Fig. 12 40 amino-acid poly-glycine. Carbons are shown in brown, Hydrogens in white, Oxygen in red and Nitrogen in light blue.

Poly-Glycine

The last system we have calculated is that of alpha-helix poly-glycine of 40 amino acids ($C_{80}H_{122}N_{40}O_{41}$). This system is also highly polar as every peptide bond along the chain contributes to the total dipole moment of the molecule. We have used norm conserving pseudopotentials of s/p cutoff radius (a.u.) of $C : 1.6/1.6$, $N : 1.5/1.5$, $O : 1.45/1.45$, and $H : 1.39$. Grid spacing of $0.4a.u.$ and a box of $20a.u. \times 20a.u. \times 160a.u.$ The system is shown in Fig. 12, this structure was not fully relaxed and the dipole can still change significantly during additional geometrical relaxation. It is calculated mostly for the comparison of CG and NG. The CG z direction (long axis) dipole was $147.4341D$, compared to $147.402D$ of NG (diff. of $\sim 0.03D$), by accident we did not fully align the molecule to the box axis and so had also dipoles in the other directions (CG/NG/diff.) $6.875D/6.866D/0.008D$ in x and $5.450D/5.449D/0.001D$ in y. The gap is already very small and with a Fermi temperature of 0.05eV the first unoccupied state was already with ~ 0.1 occupation by both calculations. The CG gap was $0.4584eV$ the NG gap was $0.4577eV$ (diff. of $0.0007eV$).

References

1 W. Koch and M. Holthausen, *A chemist's guide to density functional theory*, Wiley-VCH, 2000.

2 W. Kohn and L. J. Sham, *Physical Review*, 1965, **140**, A1133–A1138.

3 M. J. F. et al., *Gaussian 03, Revision C.02*, Gaussian, Inc., Wallingford, CT, 2004.

4 J. Izquierdo, A. Vega, L. Balbás, D. Sánchez-Portal, J. Junquera, E. Artacho, J. Soler and P. Ordejón, *Physical Review B*, 2000, **61**, 13639–13646.

5 G. Kresse, *Physical Review B*, 1996, **54**, 11169–11186.

6 M. D. Segall, P. J. D. Lindan, M. J. Probert, C. J. Pickard, P. J. Hasnip, S. J. Clark and M. C. Payne, *Journal of Physics: Condensed Matter*, 2002, **14**, 2717–2744.

7 P. Giannozzi, S. Baroni, N. Bonini, M. Calandra, R. Car, C. Cavazzoni, D. Ceresoli, G. L. Chiarotti, M. Cococcioni, I. Dabo, A. Dal Corso, S. de Gironcoli, S. Fabris, G. Fratesi, R. Gebauer, U. Gerstmann, C. Gougoussis, A. Kokalj, M. Lazzeri, L. Martin-Samos, N. Marzari, F. Mauri, R. Mazzarello, S. Paolini, A. Pasquarello, L. Paulatto, C. Sbraccia, S. Scandolo, G. Sclauzero, A. P. Seitsonen, A. Smogunov, P. Umari and R. M. Wentzcovitch, *Journal of physics. Condensed matter : an Institute of Physics journal*, 2009, **21**, 395502.

8 L. Genovese, A. Neelov, S. Goedecker, T. Deutsch, S. A. Ghasemi, A. Willand, D. Caliste, O. Zilberberg, M. Rayson, A. Bergman and R. Schneider, *The Journal of chemical physics*, 2008, **129**, 014109.

9 J. Chelikowsky, N. Troullier, K. Wu and Y. Saad, *Physical Review B*, 1994, **50**, 11355–11364.

10 J. Chelikowsky, N. Troullier and Y. Saad, *Physical review letters*, 1994, **72**, 1240–1243.

11 L. Kronik, A. Makmal, M. L. Tiago, M. M. G. Alemany, M. Jain, X. Huang, Y. Saad and J. R. Chelikowsky, *physica status solidi (b)*, 2006, **243**, 1063–1079.

12 K. Hirose, *First-principles Calculations in Real-space Formalism: Electronic Configurations and Transport Properties of Nanostructures*, World Scientific Publishing Company Pte Limited, 2005.

13 A. Castro, H. Appel, M. Oliveira, C. a. Rozzi, X. Andrade, F. Lorenzen, M. a. L. Marques, E. K. U. Gross and A. Rubio, *physica status solidi (b)*, 2006, **243**, 2465–2488.

14 T. Beck, *Reviews of Modern Physics*, 2000, **72**, 1041–1080.

15 E. Briggs, D. Sullivan and J. Bernholc, *Physical Review B*, 1996, **54**, 362–375.

16 J. R. Chelikowsky, A. T. Zayak, T.-L. Chan, M. L. Tiago, Y. Zhou and Y. Saad, *Journal of physics. Condensed matter : an Institute of Physics journal*, 2009, **21**, 064207.

17 Y. Hasegawa, J.-I. Iwata, M. Tsuji, D. Takahashi, A. Oshiyama, K. Minami, T. Boku, F. Shoji, A. Uno, M. Kurokawa, H. Inoue, I. Miyoshi and M. Yokokawa, Proceedings of 2011 International Conference for High Performance Computing, Networking, Storage and Analysis, New York, NY, USA, 2011, pp. 1:1–1:11.

18 M. Marques, *Fundamentals of Time-Dependent Density Functional Theory*, Springer, 2012.

19 M. Mundt and S. Kümmel, *Physical Review B*, 2007, **76**, 035413.

20 M. MUNDT, *Journal of Theoretical and Computational Chemistry*, 2009, **08**, 561–574.

21 Y. Saad, *Iterative Methods for Sparse Linear Systems: Second Edition*, Society for Industrial and Applied Mathematics (SIAM, 3600 Market Street, Floor 6, Philadelphia, PA 19104), 2003.

22 A. Brandt, *Mathematics of computation*, 1977, **31**, 333–390.

23 T. L. Beck, *Int. J. Quantum Chem*, 1997, **65**, 477–486.

24 A. Cerioni, L. Genovese, A. Mirone and V. A. Sole, *The Journal of chemical physics*, 2012, **137**, 134108.

25 N. D. M. Hine, J. Dziedzic, P. D. Haynes and C.-K. Skylaris, *The Journal of chemical physics*, 2011, **135**, 204103.

26 J. Jackson, *Classical Electrodynamics*, Wiley, 1998.

27 V. Rokhlin, *Journal of Computational Physics*, 1985, **60**, 187–207.

28 L. Greengard and V. Rokhlin, *J. Comput. Phys.*, 1987, **73**, 325–348.

29 S. a. Losilla, M. M. Mehine and D. Sundholm, *Molecular Physics*, 2012, **110**, 2569–2578.

30 S. a. Losilla and D. Sundholm, *The Journal of chemical physics*, 2012, **136**, 214104.

31 S. R. Jensen, J. Jusélius, A. Durdek, T. Flå, P. Wind and L. Frediani, *International Journal of Modeling, Simulation, and Scientific Computing*, 2014, **5**, 1441003.

32 W. Geng and R. Krasny, *Journal of Computational Physics*, 2013, **247**, 62–78.

33 V. Khoromskaia and B. N. Khoromskij, *Computer Physics Communications*, 2014, **185**, 3162–3174.

34 B. N. Khoromskij, V. Khoromskaia and H.-J. Flad, *SIAM Journal on Scientific Computing*, 2011, **33**, 45–65.

35 A. Kokalj, *Physical Review B*, 2011, **84**, 045418.

36 B. Delley, *The Journal of Physical Chemistry*, 1996, **100**, 6107–6110.

37 A. Boag and B. Livshitz, *IEEE Transactions on Microwave Theory and Techniques*, 2006, **54**, 3565–3570.

38 S. Li, R. Chang, A. Boag and V. Lomakin, *IEEE Antennas and Propagation Magazine*, 2012, **54**, 71–87.

39 B. Fornberg, *Mathematics of computation*, 1988, **51**, 699–706.

40 J. Han, M. L. Tiago, T.-L. Chan and J. R. Chelikowsky, *The Journal of chemical physics*, 2008, **129**, 144109.

41 A. Natan, A. Benjamini, D. Naveh, L. Kronik, M. Tiago, S. Beckman and

J. Chelikowsky, *Physical Review B*, 2008, **78**, 1–10.
42 N. A. Modine, G. Zumbach and E. Kaxiras, *Physical Review B*, 1997, **55**, 10289–10301.
43 J.-L. Fattebert, R. Hornung and A. Wissink, *Journal of Computational Physics*, 2007, **223**, 759–773.
44 A. Calzolari, N. Marzari, I. Souza and M. Buongiorno Nardelli, *Physical Review B*, 2004, **69**, 035108.
45 F. Rissner, A. Natan, D. A. Egger, O. T. Hofmann, L. Kronik and E. Zojer, *Organic electronics*, 2012, **13**, 3165–3176.
46 W.-F. Li, M. Andrzejak and H. A. Witek, *physica status solidi (b)*, 2012, **249**, 306–316.
47 C.-P. Chou, W.-F. Li, H. A. Witek and M. Andrzejak, in *Vibrational Spectroscopy of Linear Carbon Chains*, ed. L. Nemes. and S. Irle, World Scientific, 2012, ch. 12.
48 N. Troullier and J. L. Martins, *Physical Review B*, 1991, **43**, 1993–2006.
49 L. Kleinman and D. Bylander, *Physical Review Letters*, 1982, **48**, 1425–1428.
50 S. W. De Leeuw and J. W. Perram, *Molecular Physics*, 1979, **37**, 1313–1322.
51 C. A. Rozzi, D. Varsano, A. Marini, E. K. U. Gross and A. Rubio, *Physical Review B*, 2006, **73**, 205119.